The microscopic theory of fission

W. Younes and D. Gogny

Lawrence Livermore National Laboratory, Livermore, CA 94551

Abstract. Fission-fragment properties have been calculated for thermal neutron-induced fission on a ^{239}Pu target, using constrained Hartree-Fock-Bogoliubov calculations with a finite-range effective interaction. A quantitative criterion based on the interaction energy between the nascent fragments is introduced to define the scission configurations. The validity of this criterion is benchmarked against experimental measurements of the kinetic energies and of multiplicities of neutrons emitted by the fragments.

INTRODUCTION

The description of fission as a quantum many-body problem is simultaneously the most promising and the most difficult path toward a predictive theory of this phenomenon. A full treatment of all possible many-body configurations of the fissioning system is computationally unfeasible and, in many cases, unnecessary. In practice, it is known that the nucleus in its lowest-energy state is well described by a single Slater determinant. Thus, mean-field approaches such as the Hartree-Fock Bogoliubov (HFB) theory have been extremely successful in describing the fission process [1, 2, 3, 4].

A microscopic fission-theory program is being developed at the Lawrence Livermore National Laboratory which describes the fissioning system in terms of its constituent protons, neutrons, and the effective (i.e., in-medium) interaction between nucleons. This approach is based on the highly successful program developed at the Bruyères-le-Châtel laboratory over the last three decades [1, 3, 4], and provides a fully microscopic, quantum-mechanical, dynamical, and self-consistent description of fission. The only phenomenological input to the method is the effective interaction between nucleons, and the D1S finite-range interaction [6] has been used in this work.

In the first phase of the program, devoted to the static aspects of fission, we have focused on the definition and analysis of scission configurations, where the nucleus divides into (typically two) distinct fragments. The HFB formalism is the main tool used in this analysis. Static HFB calculations can be performed for specific configurations of the nucleus through the use of constraints on various collective "coordinates" of the nucleus (e.g., quadrupole/octupole/hexadecapole moments, number of particles in the neck, separation distance between fragments). Among these configurations, some will correspond to a single whole nucleus, while others will describe two distinct fragments. In this work, we will be interested in the boundary between these two regions in configuration space, and the properties of the nascent fragments (shape, kinetic and excitation energies) that can be extracted from the calculations.

THEORY

Detailed descriptions of the HFB formalism with constraints can be found in the literature [6, 7]. Here, we only recall the salient point of the theory. The lowest-energy state of the fissioning system characterized by a Hamiltonian $\hat{H}$ and a set $\{q_i\}$ of collective coordinates is found by the variational principle

$$\delta \left\langle \{q_i\} \left| \hat{H} - \lambda_N \hat{N} - \lambda_Z \hat{Z} - \sum_i \lambda_i \hat{Q}_i \right| \{q_i\} \right\rangle = 0$$

subject to the constraints

$$\langle \{q_i\} | \hat{N} | \{q_i\} \rangle = N$$
$$\langle \{q_i\} | \hat{Z} | \{q_i\} \rangle = Z$$
$$\langle \{q_i\} | \hat{Q}_i | \{q_i\} \rangle = Q_i$$

where N and Z are the neutron and proton numbers, respectively, and Q_i is any of the remaining collective-coordinate values. These collective-coordinate values are calculated as the expectation value of corresponding operators $\hat{N}$, $\hat{Z}$, and $\hat{Q}_i$. The $\hat{Q}_i$ are typically multipole operators, but we have also used the neck-size constraint

$$\hat{Q}_N \equiv \exp\left[-\frac{(z - z_N)^2}{a_N^2} \right]$$

where z is measured along the symmetry axis of the nucleus, z_N is the position of the neck (i.e., where the neck is thinnest), and $a_N = 1\,\text{fm}^2$. The many-body Hamiltonian $\hat{H}$ is expressed in terms of an effective finite-range density-dependent interaction between the nucleons with the D1S parameterization [6]. The D1S parameters were adjusted to properties of ^{16}O, ^{90}Zr, Sn isotopes, and infinite nuclear matter. The only fission-related constraint on the interaction was introduced through a slight readjustment of the surface-energy term in nuclear matter to better reproduce the height of the fission barrier in ^{240}Pu.

We have implemented the constrained HFB formalism with finite-range effective interaction in a code that uses a one-center axially deformed harmonic-oscillator basis. In this work we assume axial symmetry, and the Hamiltonian matrix assumes a block-diagonal form, with the blocks labeled by the angular-momentum projection quantum number Ω. The present calculations have been performed with up to 27 harmonic-oscillator shells in the axial direction. The two-body center-of-mass correction has been included. The Slater approximation has been used for the Coulomb-exchange interaction. Only the central part of the effective interaction has been included in the pairing interaction.

RESULTS

In this work, we have explored two distinct criteria for the definition of scission. The first definition is based on the value of Q_N, the second on the interaction energy between the
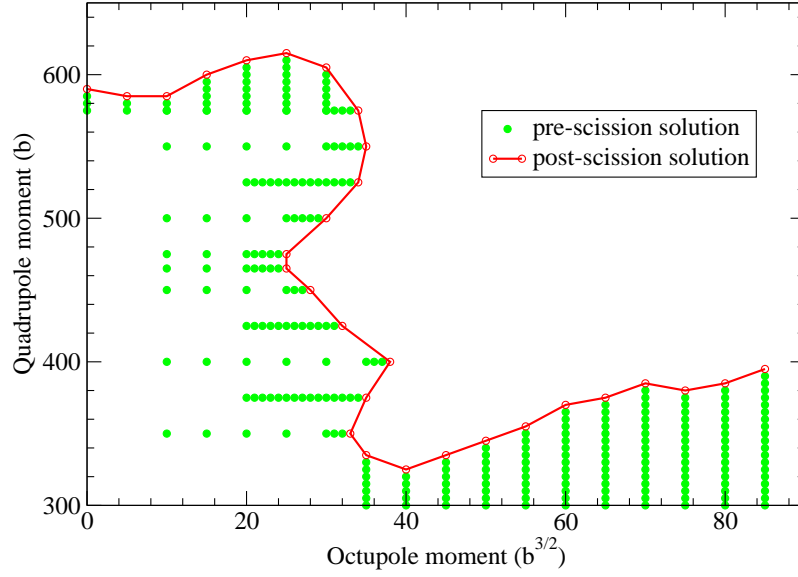
Figure 1. Scission line for ^{240}Pu hot fission obtained in this work. The solid green points represent HFB calculations producing a whole (non-scissioned) nuclear density. The empty red circles connected by a solid line represent scissioned configurations.

fragments. The scission configurations identified with a Q_N-based criterion are shown in Fig. 1 for ^{240}Pu fission.

The figure shows lines of HFB calculations at fixed Q_{20} or Q_{30} values, each using the previous solution as a starting point. The scission line was identified by a drop in Q_N to relatively small values (i.e., $Q_N \ll 0.5$) along a given line of calculations. The scission configurations identified in this manner correspond to the "hot fission" mode [1]. In this mode, the fragments are formed relatively far apart and therefore with comparatively reduced kinetic energies, and correspondingly higher excitation energies. This fission mode is expected to dominate low-energy induced fission, such as in the ^{239}Pu $\left(n_{th}, f\right)$ reaction.

The scission line obtained in Fig. 1 represents a non-trivial boundary separating regions where the nucleus is either whole or scissioned. Similarly-complicated boundaries have been previously observed by Dubray et al. [4] in their studies of Th and Fm fission. The behavior of the nucleus as it crosses the scission line is different near mass-symmetric ($Q_{30} = 0$) and most probable ($Q_{30} = 60\,\mathrm{b}^{3/2}$) fission limits. Near the symmetric limit, the variation in calculated properties (neck size, total HFB, energy, etc.) between points just before and just after the scission line is far greater than in the asymmetric case. These large variations make it impossible to extract the properties of the fragments at scission using the quadrupole and octupole constraints alone. Other constraints can be introduced, such as the hexadecapole moment Q_{40} and the neck parameter Q_N. In our analysis, we have found Q_N to be a more effective constraint to hold
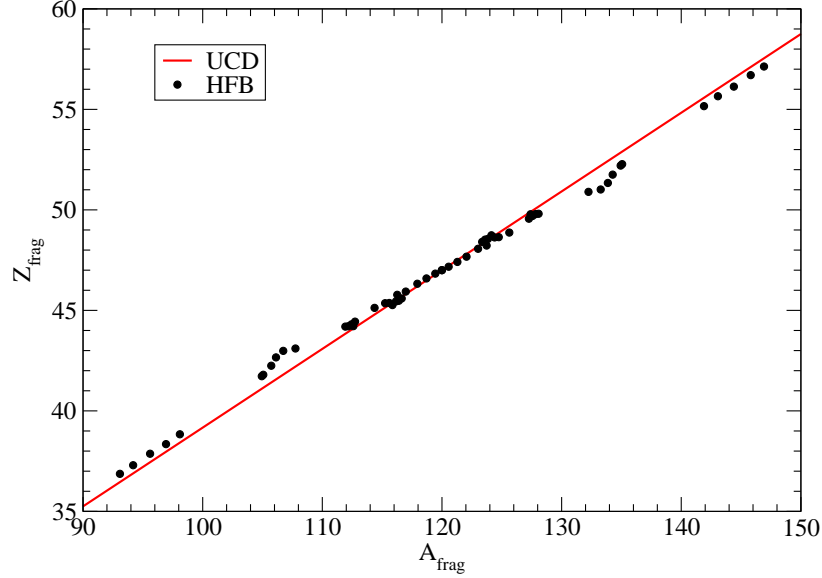
Figure 2. Fission-fragment charge number plotted as a function of mass number obtained from HFB calculations just before scission in Fig. 1. The UCD prediction (solid red line) is plotted for comparison.

the nucleus back from scission, but harder to control than Q_{40}. In addition the Q_{40} and Q_N constraints are not simply related: for a given Q_{40} value, it is possible to find distinct configurations with either a significant neck or a vanishing one [7]. For the results shown in this paper, we have used the Q_N constraint to approach the scission configurations in a more controlled manner. In the future, we plan to use both Q_N and the distance between fragments to analyze the detailed behavior of the nucleus near scission.

Using the value of Q_N as an indicator of scission, we have examined the shape properties of the nascent fragments at a point close to scission but such that the nucleus is still whole. In practice, these properties were extracted at the last (green) point along each line of calculations in Fig. 1 before the (red) scission line. In Fig. 2, we show the HFB calculations of the charge and mass numbers of the fragments at the last pre-scission point, compared to the prediction of the Unchanged Charge Distribution (UCD) model [5]. These particle numbers were obtained by integrating the proton and neutron densities to the left and right of the neck position z_N along the symmetry axis of the nucleus. The HFB and UCD predictions are in excellent agreement. This result is even more remarkable when one realizes that the only phenomenological ingredient in the HFB calculation, i.e. the effective interaction, was not explicitly adjusted to reproduce this property. Similarly, the quadrupole moment of the fragments has been extracted from the HFB calculations and, although the calculations exhibit some fluctuations, a trend emerges. As expected, the Q_{20} values drop significantly near the A = 134 mass, which is dominated by the near-spherical ^{134}Te fragment.

Despite its usefulness, the Q_N criterion for scission does present some difficulties in its

interpretation. As note before, the properties of the nucleus immediately before and after scission generally differ greatly, especially in the case of symmetric fission. Therefore, it is not clear that the kinetic and excitation energies of the fragments, which are extremely sensitive to the value of Q_N, can be correctly reproduced when adopting a criterion based on neck size. The difficulty arises because there is no objective quantitative criterion for the neck size at scission. As an alternative, we consider a definition of scission based on the interaction energy between the fragments. In order to formulate a quantitative criterion we adopt the ansatz that, in the present static calculations with constrained Q_N, scission occurs with decreasing Q_N as soon as there is enough energy available in the system to overcome the attractive part of the interaction between the fragments.

For each final (green) pre-scission point in Fig. 1, the Q_N value is progressively decreased in small increments (typically $\Delta Q_N = 0.05$). For each HFB calculation at constrained Q_N value, the single-particle wave functions are classified as either predominantly localized to the left or to the right of the neck position z_N. At this stage, the total particle densities for the left and right fragments can be readily calculated from their respective single-particle wave functions. The density for each fragment will typically exhibit a tail that extends into the complementary fragment. Often these tails can be quite large containing from a few to over a hundred nucleons in the asymmetric- and symmetric-fission limits, respectively. These tails can be reduced by a change in representation before calculating the fragment properties. In practice, for each pair of single-particle wave functions ψ_i and ψ_j within the same symmetry block in the density matrix, an angle θ is sought such that the number of particles in the tails of the rotated wave functions

$$\begin{pmatrix} \psi_i' \\ \psi_j' \end{pmatrix} = \begin{pmatrix} \cos\theta & -\sin\theta \\ \sin\theta & \cos\theta \end{pmatrix} \begin{pmatrix} \psi_i \\ \psi_j \end{pmatrix}$$

is reduced. This transformation will not yield a reduction in the tails for all possible pairs of wave functions $\left(\psi_i, \psi_j\right)$, and it is only applied to those pairs where such a reduction is achieved. All possible pair combinations are processed in this manner, and the entire procedure is iterated to suppress the tails even further. In practice, 30 iterations were sufficient to reach a decrease in tail size of less than 0.5% between subsequent iterations.

Working in this reduced-tail representation, it is now possible to calculate the interaction energy between fragments defined as

$$E_{int} = E_{HFB} - E_{HFB}(L) - E_{HFB}(R) - E_{coul}^{(D)}$$

where E_{HFB} is the HFB energy for the entire fissioning nucleus, $E_{HFB}(L)$ and $E_{HFB}(R)$ are the HFB energies of the left and right fragment respectively (calculated using the generalized densities identified for each fragment), and $E_{coul}^{(D)}$ is the direct contribution of the Coulomb energy between the fragments. Care was taken to use the density of the whole nucleus (and not that of the left or right fragment) when calculating the contribution to $E_{HFB}(L)$ and $E_{HFB}(R)$ from the density-dependent part of the interaction. The direct Coulomb term was calculated by integrating the product of fragment proton densities, folded with an inverse-distance potential. The energy E_{int} therefore contains contributions from the purely-nuclear potential as well as the attractive Coulomb-exchange term between fragments.
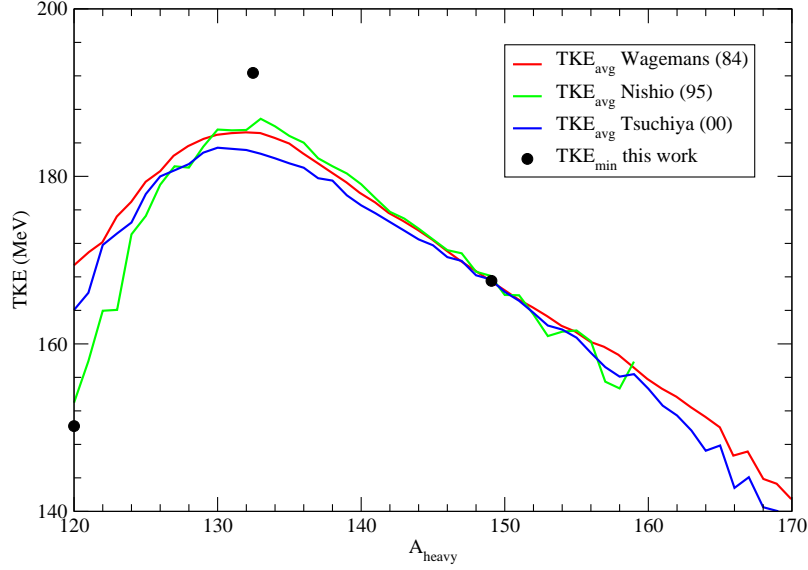
Figure 3. Comparison between measured [8, 9, 10] and calculated total kinetic energies of the fragments, plotted as a function of the heavy-fragment mass.

For low-energy fission, we assume that the energy available in the system is measured from the top of the second barrier. If $\{q\}$ denotes an arbitrary set of constraints, and $\{q_{B_{II}}\}$ the set of constraints at the second barrier, we measure the energy available in the system as $\Delta E = E_{HFB}(\{q\}) - E_{HFB}(\{q_{B_{II}}\})$. If scission is approached by varying a specific constraint, say the neck size Q_N, we then identify the scission configuration as the first instance where $\Delta E = E_{int}$. This configuration corresponds to our ansatz of building up enough energy in the system to overcome the attractive part of the interaction potential between the fragments.

Using this interaction-energy based criterion, we have calculated the kinetic and excitation energies of the fragments for a few selected points along the scission line in Fig. 1. In particular, we have made these calculations for the symmetric ($Q_{30} = 0$), most probable ($Q_{30} = 60\,\mathrm{b}^{3/2}$), and very asymmetric ($Q_{30} = 85\,\mathrm{b}^{3/2}$) fission limits. The calculated Total Kinetic Energies (TKE) are compared in Fig. 3 to three experimental measurements [8, 9, 10]. The experimental data agree everywhere, except in the symmetric-fission limit, where the measured TKE vary widely from ≈ 153 to 169 MeV. In the symmetric limit, the HFB calculations give a value for the TKE that is closest to the Nishio result, but in general, the calculated values agree with all three measurements everywhere to better than 15%. We note in particular that the calculations reproduce the observed decrease in TKE near the symmetric limit. This effect is directly related to the extreme elongation ($Q_{20} = 595\,\mathrm{b}$) reached by the nucleus at symmetric scission in Fig. 1.

In Fig. 4, we compare calculated and measured average neutron multiplicities $\nu(A)$ as a function of fragment mass. In the HFB calculations, the neutron multiplicities are obtained using the very simplistic formula

$$\nu(A) \;\; = \;\; \frac{E_x(A)}{B_n(A) + K_n}$$

where $E_x(A)$ is the excitation energy of the fragment, $B_n(A)$ is the neutron separation energy, and K_n is the average kinetic energy of the emitted neutron (taken as $K_n = 2$ MeV here). The excitation energy of each fragment was calculated as the difference between HFB energies of the system at scission (obtained in this work) and in its ground state (taken from the AMEDEE database of ground-state HFB calculations [11]). Because the two-body center-of-mass contribution is calculated for the fissioning nucleus, a correction (of order ~ 3 MeV) was applied to the excitation energy of individual fragments to restore the appropriate center-of-mass energy for that fragment. The neutron-multiplicity data exhibit a great deal of variability near symmetric fission, as well as for heavy asymmetric fragments. Nevertheless, the calculations are in excellent agreement with the data, except perhaps near the symmetric limit. The most recent data, from Batenkov et al. [12], indicate a sharp rise up to $\nu \approx 4.4$ near $A = 117$, not far from the $\nu \approx 4.1$ near $A = 120$ found in the present calculation. However, the remaining data [9, 10, 13] and Wahl evaluation [5] peak at a lower value of 2.3-3.2 near $A = 114$, albeit with significant experimental uncertainties. On the other hand, the dip in multiplicity around the nearly-spherical $A = 130$ fragments is well reproduced by the calculations.

CONCLUSION

In this work, we have calculated fission-fragment properties for the ^{239}Pu $\left(n_{th}, f\right)$ reaction in a fully microscopic approach using static constrained HFB calculations with a finite-range interaction. Near scission, we have separated the Slater-determinant HFB solution into an *anti-symmetrized* product of two distinct Slater determinants, one corresponding to each fragment. We have introduced a quantitative criterion to identify scission configurations based on building up a sufficient amount of available energy in the fissioning system to overcome the attractive part of the interaction between the fragments. Using this criterion, we have calculated the kinetic and excitation energies of the fragments and found them to be in very good agreement with experimental data. In the future, we will extend the calculations of fragment properties to more points along the scission line in Fig. 1 and analyze the approach to scission as a function of the distance between fragments. We will also explore the impact on these properties of a full dynamical treatment of fission, using the approach developed in [1, 3].
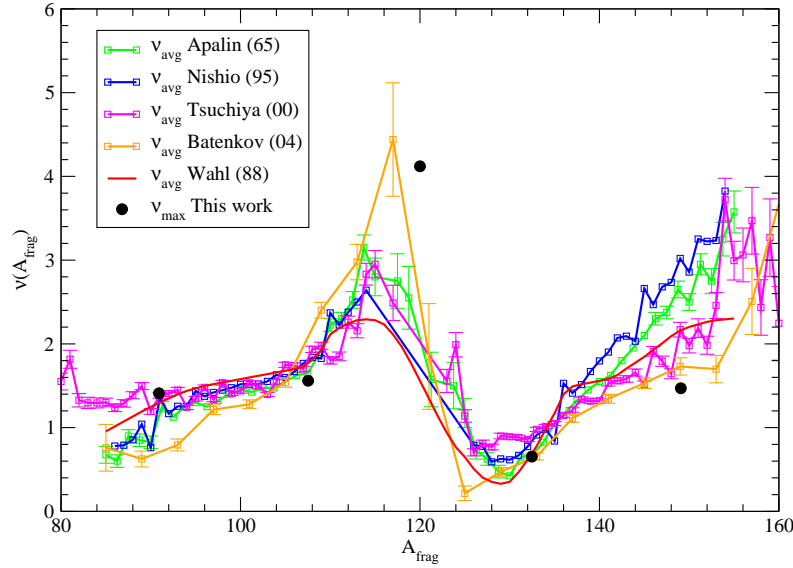
ACKNOWLEDGMENTS

Figure 4. Comparison between measured [9, 10, 12, 13] and calculated average neutron multiplicities, plotted as a function of fragment mass.

REFERENCES

1. J.-F. Berger, M. Girod, and D. Gogny, Nucl. Phys. **A428**, 23 (1984).
2. M. Warda, J. L. Egido, L. M. Robledo, and K. Pomorski, Phys. Rev. C **66**, 014310 (2002).
3. H. Goutte, J.-F. Berger, P. Casoli, and D. Gogny, Phys. Rev. C **71**, 024316 (2005).
4. N. Dubray, H. Goutte, and J.-P. Delaroche, Phys. Rev. C **77**, 014310 (2008).
5. A. C. Wahl, At. Data Nucl. Data Tables **39**, 1 (1988).
6. J. Dechargé and D. Gogny, Phys. Rev. C **21**, 1568 (1980).
7. W. Younes and D. Gogny, submitted to Phys. Rev. C (2009).
8. C. Wagemans, E. Allaert, A. Deruytter, R. Barthélémy, and P. Schillebeeckx, Phys. Rev. C **30**, 218 (1984).
9. K. Nishio, Y. Nakagome, I. Kanno, and I. Kimura, J. Nucl. Sci. Tech. **32**, 404 (1995).
10. C. Tsuchiya, Y. Nakagome, H. Yamana, H. Moriyama, K. Nishio, I. Kanno, K. Shin, and I. Kimura, J. Nucl. Sci. Tech. **37**, 941 (2000).
11. S. Hilaire and M. Girod, "Hartree-Fock-Bogoliubov results based on the Gogny force", http://www-phynu.cea.fr/science_en_ligne/carte_potentiels_microscopiques/carte_potentiel_nucleaire_eng.htm
12. O. A. Batenkov, G. A. Boykov, F.-J. Hambsch, J. H. Hamilton, V. A. Jakovlev, V. A. Kalinin, A. B. Laptev, V. E. Sokolov, and A. S. Vorobyev, in Proceedings of the Intl. Conf. on Nucl. Data for Sci. and Tech., AIP Conf. Proc. **769**, 1003 (2004).
13. V. F. Apalin, Yu. N. Gritsyuk, I. E. Kutikov, V. I. Lebedev, L. A. Mikaelian, Nucl. Phys. **71**, 553 (1965).